

See discussions, stats, and author profiles for this publication at: <https://www.researchgate.net/publication/231223160>

Hydrogen Bonding between the Q(B) Site Ubisemiquinone and Ser-L223 in the Bacterial Reaction Center: A Combined Spectroscopic and Computational Perspective

ARTICLE *in* BIOCHEMISTRY · SEPTEMBER 2012

Impact Factor: 3.02 · DOI: 10.1021/bi300834w · Source: PubMed

CITATIONS

9

READS

18

7 AUTHORS, INCLUDING:



Tzu-Jen Lin

Academia Sinica

8 PUBLICATIONS 114 CITATIONS

SEE PROFILE



Rimma I Samoilova

Russian Academy of Sciences

77 PUBLICATIONS 843 CITATIONS

SEE PROFILE



Patrick J O'Malley

The University of Manchester

47 PUBLICATIONS 705 CITATIONS

SEE PROFILE

Hydrogen Bonding between the Q_B Site Ubisemiquinone and Ser-L223 in the Bacterial Reaction Center: A Combined Spectroscopic and Computational Perspective

Erik Martin,^{†,@} Amgalanbaatar Baldansuren,[‡] Tzu-Jen Lin,[§] Rimma I. Samoilova,^{||} Colin A. Wraight,^{*,†,⊥} Sergei A. Dikanov,^{*,‡} and Patrick J. O'Malley^{*,§}

[†]Center for Biophysics and Computational Biology, University of Illinois at Urbana-Champaign, Urbana, Illinois 61801, United States

[‡]Department of Veterinary Clinical Medicine, University of Illinois at Urbana-Champaign, Urbana, Illinois 61801, United States

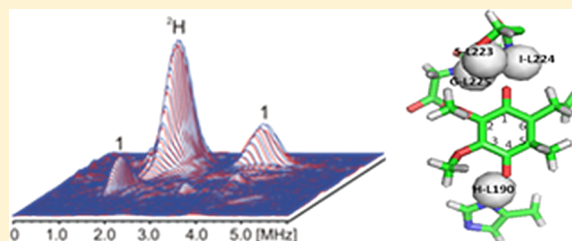
[§]School of Chemistry, University of Manchester, Manchester M13 9PL, U.K.

^{||}Institute of Chemical Kinetics and Combustion, Russian Academy of Sciences, Novosibirsk 630090, Russian Federation

[⊥]Department of Biochemistry, University of Illinois at Urbana-Champaign, Urbana, Illinois 61801, United States

S Supporting Information

ABSTRACT: In the Q_B site of the *Rhodobacter sphaeroides* photosynthetic reaction center, the donation of a hydrogen bond from the hydroxyl group of Ser-L223 to the ubisemiquinone formed after the first flash is debatable. In this study, we use a combination of spectroscopy and quantum mechanics/molecular mechanics (QM/MM) calculations to comprehensively explore this topic. We show that ENDOR, ESEEM, and HYSCORE spectroscopic differences between mutant L223SA and the wild-type sample (WT) are negligible, indicating only minor perturbations in the ubisemiquinone spin density for the mutant sample. Qualitatively, this suggests that a strong hydrogen bond does not exist in the WT between the Ser-L223 hydroxyl group and the semiquinone O₁ atom, as removal of this hydrogen bond in the mutant should cause a significant redistribution of spin density in the semiquinone. We show quantitatively, using QM/MM calculations, that a WT model in which the Ser-L223 hydroxyl group is rotated to prevent hydrogen bond formation with the O₁ atom of the semiquinone predicts negligible change for the L223SA mutant. This, together with the better agreement between key QM/MM calculated and experimental hyperfine couplings for the non-hydrogen-bonded model, leads us to conclude that no strong hydrogen bond is formed between the Ser-L223 hydroxyl group and the semiquinone O₁ atom after the first flash. The implications of this finding for quinone reduction in photosynthetic reaction centers are discussed.



The primary event in photosynthesis is light-driven charge separation, catalyzed by the reaction center (RC) protein–pigment complex. Light activation results in the transfer of an electron from the primary donor, P, a dimer of (bacterio)chlorophyll, through a series of low-potential cofactors. On time scales longer than a nanosecond, the charge separation in RCs from purple bacteria resides on the primary donor and on the acceptor quinones. The primary quinone, Q_A, is tightly bound and functions as a one-electron redox species, transferring electrons sequentially to the secondary quinone, Q_B. This secondary quinone, Q_B, is reversibly bound and can be doubly reduced via the semiquinone (SQ) form of Q_A (SQ_A or Q_A^{•−}, depending on context) with the uptake of two protons. The fully reduced, protonated quinol is released and replaced by another quinone (reviewed in refs 1 and 2). The purple bacterial RC therefore uses light energy to produce reduced ubiquinol, which is then used as a substrate by the cytochrome *bc*₁ complex. This creates the proton electrochemical gradient needed for the production of ATP from ADP. In the Q_B binding site, the two neutral forms, quinone and quinol, are weakly bound, but the negatively charged semiquinone free

radical intermediate, SQ_B or Q_B^{•−}, is tightly bound and stabilized. Hydrogen bonding by the SQ oxygen atoms to nearby amino acid donor groups can be expected to contribute significantly to its stability. Hydrogen-bonded residues are also likely to be the immediate source of protons for reduction of the quinone to the quinol form. Ubiquinol is also the substrate for cytochrome *bc*₁ in the respiratory electron transfer chain where it is generated by reduction in Complexes I and II.³ Photosystem II in cyanobacteria, algae, and higher plants uses a mechanism similar to that of the purple bacterial reaction center to reduce plastoquinone to plastoquinol, which is the substrate for the cytochrome *b*₆*f* complex.

Quinone substrate binding sites such as Q_B are often difficult to characterize experimentally as such sites will have low occupancy because of the binding and unbinding of the substrate and product. Of the quinone reduction sites, the Q_B

Received: June 21, 2012

Revised: September 24, 2012

Published: September 27, 2012

site in the bacterium *Rhodobacter sphaeroides* is the best characterized by experimental methods. High-resolution X-ray crystal structures of the site are available,^{4–6} and a wide range of spectroscopic methods such as EPR⁷ and FTIR⁸ have been used to examine the quinone and semiquinone forms. Details of putative hydrogen bond donors have been elucidated from the structural data, and mechanisms of protonation to the ubiquinol have been proposed.⁹ Crystal structures show Q_B can occupy at least two different configurations, a tightly bound proximal position and a distal position more distant from the $Fe^{II}-(His)_4$ complex.^{6,10} Q_B is always seen to occupy the proximal location in preparations in which the RC was frozen under illumination, indicating that it is this conformation that traps the semiquinone (SQ_B) state. Structures with Q_B in the proximal position show the HN_δ group of His-L190 (an Fe ligand) as a potential hydrogen bond donor to the carbonyl oxygen O_4 , and backbone NH groups from Ile-L224 and/or Gly-L225 and the hydroxyl group of Ser-L223 as potential hydrogen bond donors to the carbonyl O_1 atom (Figure 1).

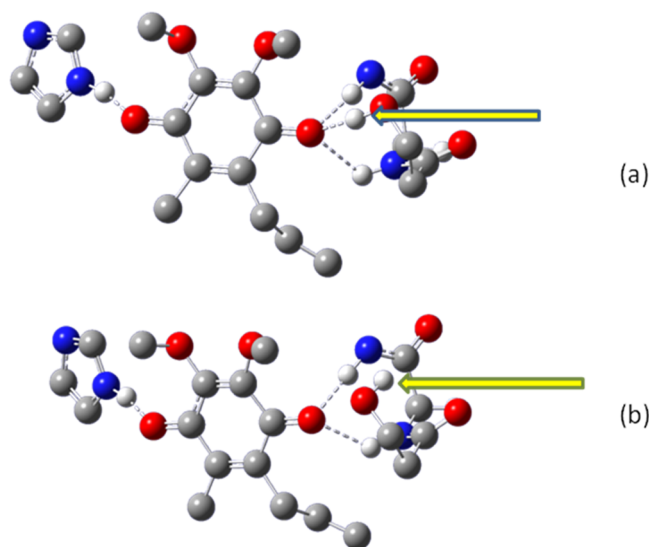


Figure 1. Optimized Q_B site model for (a) WT-HB and (b) WT-NHB. In panel a, the donation of a hydrogen bond to the O_1 atom occurs from the peptide NH groups of Gly-L225 and Ile-L224 and the hydroxyl group of Ser-L223. In panel b, the Ser-OH group does not donate a hydrogen bond to the O_1 atom. Arrows point to the position of the Ser-L223 hydroxyl group hydrogen atom.

The donation of a hydrogen bond from the hydroxyl group of Ser-L223 is debatable, with reports appearing for and against the presence of such a hydrogen bond to O_1 of the quinone or the semiquinone. Early reports, allied to the initial crystal structures, were supportive of such a H-bond,⁶ and electrostatic calculations suggested that the Ser-L223 hydroxyl group would be hydrogen bonded to the ionized side chain of Asp-L213 in the ground state (oxidized Q_B) but switch to the anionic semiquinone, Q_B^- .¹¹ However, subsequent FTIR studies¹² argued against the significant formation of H-bonds to either the quinone ($Q_A Q_B$) or semiquinone ($Q_A Q_B^-$) state. Nevertheless, this interaction is believed to be a key factor for the eventual protonation of the semiquinone leading to formation of the fully reduced quinol, and recent ENDOR studies¹³ have appeared to show Ser-L223 hydrogen bonding to the Q_B semiquinone in the $Q_A Q_B^-$ state. This would favor the model in which the Ser-L223 hydroxyl group acts initially as a H-bond

donor to Asp-L213 when the quinone form is present in the site, but upon reduction to the SQ state after a single flash, rotation of the hydroxyl group is proposed to lead to formation of a hydrogen bond to the O_1 atom of the SQ .

In this report, we examine the effects of replacing the Ser-L223 residue with Ala, generating the L223SA mutant. Alanine will not hydrogen bond with the quinone or semiquinone O_1 atom, and therefore, changes to the EPR spectroscopic properties would be expected in the mutant if the Ser-L223 residue did form a strong hydrogen bonding interaction with the O_1 atom in the wild type (WT). We use ENDOR and ESEEM spectroscopies to probe any differences that exist between the WT and L223SA mutant. We also model the mutation using QM/MM calculations allowing us to quantitatively calculate any changes that should occur for comparison with the experimental determinations.

■ EXPERIMENTAL PROCEDURES

Reaction Center Mutation and Expression. The serine L223 to alanine (L223SA) mutation was introduced by standard procedures for site-directed mutagenesis, based on Stratagene's QuikChange method (Stratagene, La Jolla, CA), as previously described.^{14,15} The mutant was constructed in the complementation vector, pLMX415His6, which contains an engineered reaction center operon (*puf*) lacking *pufA* and *pufB* of light-harvesting complex 1 (LH1), with a hexahistidine tag at the C-terminus of subunit M. pLMX415His6 is derived from the broad host-range plasmid pRK415 and was transferred from *Escherichia coli* strain S17-1 into *Rba. sphaeroides* by conjugation. The expression strain, GaBM, was derived from the green Ga parent and lacked RCs and both light-harvesting pigment complexes (LH1 and LH2).¹⁵ Cells were grown heterotrophically on Sistrom's minimal medium with malate, in the dark, and with 2 μ g/mL tetracycline. Pigmentation was induced by the transition to semiaerobic conditions. For reaction center isolation, cell membranes were solubilized in 1% lauryldimethylamine-*N*-oxide (LDAO) and purified using nickel affinity chromatography, essentially as described previously.¹⁶

Sample Preparation. To isolate SQ EPR signals, the native, high-spin Fe^{2+} must be replaced by diamagnetic Zn^{2+} . Procedures for biochemical metal exchange, along with the methods of bacterial cell growth and RC isolation, were as previously described.¹⁷ ^{15}N enrichment of RCs was accomplished during cell growth by using ^{15}N -labeled ammonium sulfate (Cambridge Isotopes) in minimal growth medium. Prior to EPR sample generation, the detergent, LDAO, used in RC isolation, was exchanged for Triton X-100 by dilution of approximately 100-fold in 10 mM Tris [pH (pD) 7.9], 20 μ M EDTA, and 0.03% Triton X-100 and reconcentration. The same method was used for deuterium-exchanged samples, by dilution in D_2O buffer and incubation for 24 h before reconcentration. Samples with Q_A^- were made by chemical reduction with 8 mM sodium dithionite. For samples with Q_B^- , the RCs were combined with a 3-fold excess of both ubiquinone-50 (Q_{10}) and cytochrome *c*, reduced in 10 mM ascorbate. To trap the Q_B SQ , the sample was illuminated by a single laser flash at 532 nm (Spectra Physics Quanta-Ray GCR-11 Nd:YAG laser) and immediately frozen in liquid nitrogen. A routine optical assay of Fe/Zn-exchanged RC preparations showed a minimum of 80% reconstitution of Q_B activity. However, pulsed EPR measurements showed no sign of Q_A SQ signals in Q_B SQ samples in either 1H HYSCORE or ^{14}N or

Table 1. Calculated ^{13}C , ^{17}O , and ^1H Hyperfine Couplings (Megahertz) for Q_B Site Hydrogen Bonding Interactions in WT and the L223SA Mutant Model

position	WT-HB		L223SA		WT-NHB	
	anisotropic	isotropic	anisotropic	isotropic	anisotropic	isotropic
	T_{33}, T_{22}, T_{11}	a	T_{33}, T_{22}, T_{11}	a	T_{33}, T_{22}, T_{11}	a
$^{13}\text{C}_1$	30.6	3.3	25.2	−1.5	25.2	−1.7
	−16.6		−14.1		−14.0	
	−14.0		−11.1		−11.2	
$^{13}\text{C}_4$	26.3	1.0	28.3	2.3	29.2	3.6
	−14.4		−15.4		−15.4	
	−11.9		−12.9		−13.0	
$^{17}\text{O}_1$	−66.9	−18.3	−71.6	−18.4	−72.1	−18.3
	−33.6		38.0		35.6	
	−33.3		37.1		36.5	
$^{17}\text{O}_4$	−62.6	−18.2	−61.6	−17.8	−60.5	−17.9
	31.4		30.3		29.9	
	31.2		29.7		30.5	
$^1\text{H CH}_3(\text{S}')$	2.6	7.6	2.6	5.6	2.5	5.8
	−1.7		−1.6		−1.6	
	−1.0		−1.0		0.9	

^{15}N HYSCORE spectra, indicating that the functional reconstitution was complete, probably because of the much higher concentrations involved.

EPR, ENDOR, and ESEEM Experiments. The instrumentation for X-band and Q-band CW EPR measurements was as previously described.¹⁸ The instrumentation, pulse sequences, and spectral processing for X-band one-dimensional four-pulse ESEEM ($\pi/2-\tau-\pi/2-t-\pi-t-\pi/2$ -echo) and two-dimensional four-pulse ESEEM (HYSCORE) ($\pi/2-\tau-\pi/2-t_1-\pi-t_2-\pi/2$ -echo) were also as previously described.¹⁸ Pulsed ENDOR spectra of the semiquinones were obtained using Davies ($\pi-t-\pi/2-\tau-\pi-\tau$ -echo) and Mims ($\pi/2-\tau-\pi/2-t-\pi/2-\tau$ -echo) sequences with different pulse lengths. In addition, a radiofrequency π pulse was applied during time interval t in both sequences. The specifics of these experiments are described in detail elsewhere.¹⁹

Computational Studies. Starting with the *Rba. sphaeroides* structure of Axelrod et al.²⁰ (Protein Data Bank entry 1dv3), we created a model of the Q_B site. This model consisted of L subunit residues 177–242 and M subunit residues 218–220, 233–235, and 265–267 and the non-heme Fe^{2+} . Hydrogens were added, and the native Fe^{2+} ion was replaced with Zn^{2+} . The ubiquinone isoprene chain was reduced to CH_2CHCH_2 . For the optimization studies, two-layer ONIOM calculations [ONIOM(B3LYP/6-31G(d):UFF)] were performed. The QM layer contained ubisemiquinone Q_B , His-L190, Gly-L225, Ile-L224, Ser-L223, Zn, and its other ligands. The remaining atoms formed the MM layer. Linking between the QM and MM layers was achieved using hydrogen link atoms. Keeping all heavy atoms except the semiquinone fixed, we optimized the semiquinone geometry within the site. All hydrogen atom positions were optimized. In one model, WT-HB, the hydroxyl group of the Ser-L223 residue was initially positioned within hydrogen bonding distance of the quinone O_1 atom. In a second model, WT-NHB, it was rotated away from hydrogen bonding range. To model the L223SA mutant, the CH_2OH group of Ser-L223 in the WT models was replaced with a methyl group. Charges for the MM layer were generated using the qEq method and electrostatic embedding; i.e., ONIOM-EE was employed.²¹ This geometry was then used in a further

single-point ONIOM (B3LYP/EPR-II:UFF) calculation to obtain spin densities and hyperfine coupling constants (hfcs). For the Zn atom, the 6-31G(d) basis set was used. All calculations were performed using Gaussian 09.²²

RESULTS AND DISCUSSION

^1H ENDOR studies of semiquinones have proven to be very successful in measuring hyperfine couplings to rotating methyl groups and hydrogen-bonded protons.⁷ Strong ENDOR responses are seen for both types of protons. For the ubisemiquinone free radical, the S' -methyl group ^1H hfc is directly proportional to the unpaired spin density at the C_5 position and is an excellent probe of the spin density distribution around the ring. In quinone binding sites or in protic solvents, changes in the spin density distribution of the ring are caused by the donation of hydrogen bonds to the O_1 and O_4 atoms. Using density functional theory calculations, it was shown that the formation of hydrogen bonds to the oxygen atoms of the semiquinone leads primarily to a redistribution of spin density from the oxygens to the C_{ipso} atom.^{23,24} The increased spin density at the C_{ipso} atom can then lead via spin polarization to a decreased spin density at the neighboring ortho carbon atoms. This will in turn, via a secondary spin polarization mechanism, lead to an increased π spin density at the meta positions. The extent of this redistribution of spin density is directly proportional to both the strength and number of hydrogen bonds formed. For a symmetrical hydrogen bonding situation with equal hydrogen bonding to both O_1 and O_4 , one observes decreased O spin density and increased C_{ipso} spin density, and this is the situation that usually exists in protic solvents. In protein binding sites, however, different strengths and/or quantities of hydrogen bonds can occur for the O_1 and O_4 atoms. If hydrogen bonds are formed to only one oxygen atom, this is manifested in an asymmetric spin density for the SQ_B as demonstrated by the phylosemiquinone present in Photosystem I.^{25,26} For example, if a hydrogen bond is donated only at the O_4 atom, this will lead to enhanced spin density at the C_4 , C_6 , C_2 , and O_1 atoms with corresponding decreases at O_4 , C_3 , C_5 , and C_1 . This would be reversed for the formation of a hydrogen bond to only O_1 .

Table 2. Calculated ^1H and ^{14}N Hyperfine Couplings (Megahertz) for Q_B Site Hydrogen Bonding Interactions in the WT and L223SA Mutant

position	WT-HB		L223SA		WT-NHB	
	anisotropic	isotropic	anisotropic	isotropic	anisotropic	isotropic
	T_{33}, T_{22}, T_{11}	a	T_{33}, T_{22}, T_{11}	a	T_{33}, T_{22}, T_{11}	a
^1HN His-L190	10.2	−0.4	10.7	−0.2	10.3	−0.1
	−5.3		−5.6		−5.4	
	−4.9		−5.1		−4.9	
^1HN Gly-L225	6.6	−0.6	7.3	−0.7	8.4	−0.8
	−3.7		−4.0		−4.5	
	−2.9		−3.3		−3.8	
^1HN Ile-L224	3.9	−0.1	5.0	−0.2	4.9	−0.1
	−2.1		−2.6		−2.6	
	−1.8		−2.3		−2.3	
^1HO Ser-L223	7.6	−0.8			1.8	0.0
	−4.0				−1.0	
	−3.7				−0.8	
$^{14}\text{N}_\delta$ His-L190	0.4	1.5	0.4	1.4	0.4	1.4
	−0.2		−0.2		−0.2	
	−0.2		−0.2		−0.2	
^{14}NH Gly-L225	0.3	0.6	0.3	0.6	0.3	0.9
	−0.2		−0.2		−0.2	
	−0.1		−0.1		−0.1	
^{14}NH Ile-L224	0.2	0.1	0.2	0.2	0.2	0.1
	−0.1		−0.1		−0.1	
	−0.1		−0.1		−0.1	

Usually, rather than exclusive hydrogen bonding to only one side, there is a difference in the extent and strength of hydrogen bonds formed to the two oxygens leading to a situation intermediate between the extremes described above. For the Q_B site in *Rba. sphaeroides*, X-ray crystal structure data^{5,10} have shown that the O_4 atom is a potential acceptor of a hydrogen bond from the N_δH group of His-L190. The O_1 atom is a potential acceptor of a hydrogen bond from the peptide NH groups of Gly-L225 and Ile-L224 and the Ser-L223 OH group. Because of its rotational freedom, the Ser-L223 hydroxyl group can be rotated away from hydrogen bond donation to O_1 , and indeed, in some models it has been proposed to hydrogen bond to Asp-L213 instead.^{11,12} On the basis of the previous report of a hydrogen bond to Ser-L223 by Q-band ENDOR,¹³ we assumed in a previous publication¹⁸ that the hydroxyl group of this residue is rotated such that a hydrogen bond is donated to the SQ_B O_1 atom. This hydrogen-bonded model is denoted WT-HB. In this study, we additionally look at an alternative model (WT-NHB) in which the Ser-L223 hydroxyl group is rotated away from the SQ_B atom, thereby preventing the donation of a hydrogen bond to the SQ_B O_1 atom. The calculated values for WT-NHB are listed in Table 1 and compared with those obtained with the hydrogen-bonded model, WT-HB. The changes in calculated hyperfine couplings are as expected from our qualitative discussion given above. Removal of the hydrogen bond from the Ser-L223 hydroxyl leads to an increase in the magnitudes of the O_1 , C_2 , C_6 , and C_4 anisotropic hfc's, with a corresponding reduction in the O_4 , C_5 , C_3 , and C_1 values. As the anisotropic hyperfine coupling magnitudes are a direct measure of the π spin density at these atom positions, this also reflects the spin density changes.

In a previous publication,¹⁸ we pointed out the poor agreement between the ^1H isotropic hfc of the 5'-methyl group for the WT-HB model (7.3 MHz) and the experimental

value (5.4 MHz). This was surprising as this hfc is one of the most accurately calculated for the Q_A site and other semiquinone sites. We now believe that this discrepancy was due to the use of the WT-HB model for this calculation. The extra hydrogen bond from the hydroxyl of Ser-L223 to the SQ_B O_1 leads, as explained above, to an elevated spin density value at the C_5 position. This leads in turn to a larger ^1H hfc for the 5'-methyl group. The absence of the Ser-L223 hydrogen bond in the WT-NHB model accounts for the smaller C_5 spin density value with a resultant smaller ^1H isotropic hfc of 5.8 MHz for the methyl group, which is in better quantitative agreement with the experimental value of 5.4 MHz. It is also of particular note from Table 1 that the calculated ^{13}C A_{zz} ($a + T_{33}$) value for C_4 of the WT-NHB model (32.8 MHz) is larger than the value of 23.5 MHz calculated for the corresponding A_{zz} of C_1 . For the WT-HB model, the calculations show the opposite, with a larger A_{zz} value for C_1 of 33.1 MHz compared with a C_4 value of 27.3 MHz. Experimental EPR spectra clearly support the larger A_{zz} of the C_4 (32.2 MHz) hyperfine coupling versus that of C_1 (27.7 MHz). The extra hydrogen bond to O_1 introduced from Ser-L223 in the WT-HB model is calculated to flip the spin density polarization over to a situation in which C_1 has the larger value, in clear disagreement with the experimental observations.

The calculated hfcs for the L223SA mutant model are also listed in Tables 1 and 2. These are significantly different from those of the WT-HB model but are practically unchanged from those calculated for the WT-NHB model. The QM/MM calculations therefore predict an identical spin density distribution for the WT-NHB and L223SA models. For the mutant, the calculated ^1H isotropic hfc value for the 5'-methyl group of 5.6 MHz is very close to the WT-NHB model value of 5.8 MHz. The experimental pulsed ^1H ENDOR spectra, in both protonated and deuterated solutions, for mutant and WT

models are overlaid in Figure 2. The spectra are essentially identical. The D₂O solvent preparations show intense bands

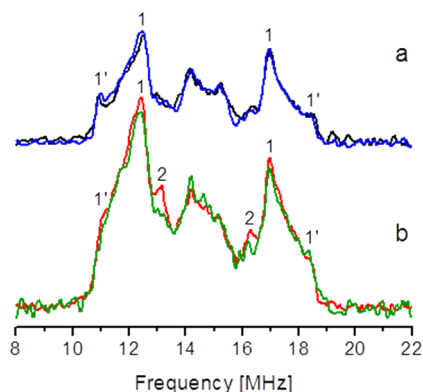


Figure 2. Pulsed ¹H ENDOR spectra of SQ_B in WT (black) and L223SA (blue) in ²H₂O and of SQ_B in WT (red) and L223SA (green) RCs in ¹H₂O. The spectra were measured using the Davies pulse sequence (π - t - $\pi/2$ - τ - π -echo) with a radiofrequency (RF) π pulse applied during time interval t with the following: lengths of microwave pulses (t_{MW}) of 88, 44, and 88 ns, τ of 380 ns, length of RF pulse of 16 μ s, MW frequency of 9.690 GHz, temperature of 70 K.

with well-pronounced features defining parallel (1') and perpendicular (1) principal values of 7.8 (1') and 4.4 MHz (1), respectively, for the axial hyperfine tensor of the 5'-methyl protons. These principal values determine the isotropic hyperfine constant of ~5.5 MHz. Identical values are observed for the mutant sample showing that, experimentally, no change in the value of this coupling is observed. If a hydrogen bond were present from the Ser-L223 hydroxyl group to the O₁ atom of SQ_B in the WT, the QM/MM calculated values discussed above indicate that the 5'-methyl hfc should change significantly and be clearly evident in the spectra of Figure 2a. The unchanged position of these bands in the L223SA spectrum signifies that Ser-L223 is not hydrogen bonded to the O₁ atom of SQ_B in the WT.

In addition, it is instructive to look for direct evidence of hydrogen bonding via the presence of ENDOR bands due to the hydrogen-bonded protons. As mentioned above, these usually give rise to strong ¹H ENDOR signals, and if such a hydrogen bond exists from the Ser-L223 hydroxyl group in the WT, it will be absent in the L223SA spectrum. The QM/MM calculations for the hydrogen-bonded WT-HB model (Table 2) indicate that large hyperfine coupling values for the parallel component of 6.8 MHz and the perpendicular component of 4.5–4.7 MHz are expected for the Ser-L223 hydrogen bond interaction. The absence of this interaction in the mutant should be clearly visible via comparison of the protonated solvent WT and mutant spectra (Figure 2b). The overlap of the WT and L223SA spectra in Figure 2b shows no major differences. Some minor intensity changes are noted, especially the features (2) corresponding to a splitting of ~3 MHz, which we ascribe to small rearrangements of the Q_B binding site after the mutation. In the Supporting Information, four-pulse ESEEM, showing sum-combination peaks, and ²H HYSCORE spectra are shown to be similar for both WT and L223SA samples and further support the absence of Ser-L223 hydrogen bonding in WT. The four-pulse X-band ¹H spectra are mostly sensitive to the anisotropic hyperfine couplings. The similarity of the spectra in WT and mutant samples indicates that

anisotropic couplings are not responsible for the features (2) in ENDOR spectra. Therefore, one can suggest that the observed difference results from small variations in the isotropic hyperfine coupling of one or more of the hydrogen bond protons. The QM/MM calculations (Table 2) do show that the Gly-L225 ¹H values are slightly lower for the mutant than for the WT-NHB model. This is presumably linked to the slightly longer Gly-L225 H-bond distance calculated for the mutant model and shown in Table 3.

Table 3. SQ_B Optimized Carbonyl Covalent Bond and Hydrogen Bond Distances^a

bond	WT-HB	WT-NHB	L223SA
C ₄ -O ₄	1.28	1.28	1.28
C ₁ -O ₁	1.28	1.27	1.28
O ₄ -HN _δ His-L190	1.58	1.55	1.54
O ₁ -HN Gly-L225	2.00	1.83	1.91
O ₁ -HO Ser-L223	1.81 (2.80)	3.10 (2.85)	—
O ₁ -HN Ile-L224	2.30	2.10	2.10

^aThe O₁-Ser O distance is given in parentheses. All distances in angstroms.

In addition to the ENDOR studies described above, we have also conducted ¹⁴N and ¹⁵N HYSCORE studies on both WT and L223SA mutant samples. Figures 3 and 4 show comparison of the ¹⁴N and ¹⁵N HYSCORE spectra in WT and mutant samples. The ¹⁴N spectra consist of two pairs of cross-peaks 1 and 2 produced by the HN_δ group of His-L190 and the peptide NH group of Gly-L225, respectively.^{17,18} There is essentially no visible difference between ¹⁴N spectra. The ¹⁵N spectra also show cross-peaks 1 and 2 from the same nitrogens and an additional narrow peak (3) at the diagonal point (¹⁵N_N, ¹⁵N_N) from other weakly coupled nitrogens.^{17,18} Some differences between the WT and mutant are seen in the ¹⁵N HYSCORE spectra, notably the larger width of the cross-peaks (1) from the His nitrogen and the greater intensity of the diagonal peak (3). The change in line shape (1) may be due to a slight change of the coupling or rhombicity of the anisotropic hyperfine tensor. The change in the diagonal peak (3) intensity may indicate reorganization of the protein environment induced by the mutation, effectively decreasing the average distance from SQ_B to the nearest nitrogens. The lack of any significant difference in ¹⁴N and ¹⁵N hyperfine couplings between the WT and L223SA is in agreement with the QM/MM calculations of these parameters in Table 1, which shows essentially no change in the calculated values of these couplings for all three models.

The results of this work, showing no strong hydrogen bonding between Ser-L223 and Q_B⁻ in the Q_AQ_B⁻ state, are in apparent contrast with the CW-ENDOR study by Paddock et al.²⁷ Their conclusions were based purely on the observation of ¹H ENDOR intensity changes, on mutation, which were attributed directly to hydrogen-bonded proton hyperfine couplings from the L223-Ser hydroxyl group in the WT sample. As mentioned above, we do observe some intensity changes in this hydrogen bonding region upon mutation but not as extensively as reported in the other study. They did not report any ¹H hyperfine coupling values for the 5'-methyl group, which is a clearer indicator of the hydrogen bonding status of the SQ. In addition, the main results in their study were obtained with an extensively mutated reaction center, in which Q_A is missing because of the positioning of a mutant tryptophan residue in the quinone binding site. In the case of

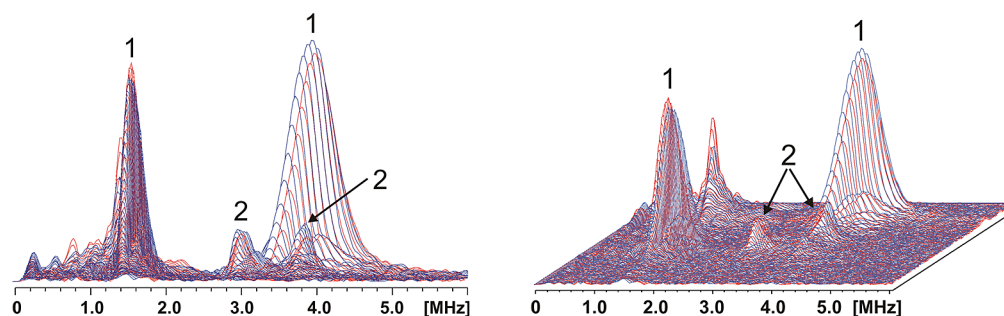


Figure 3. Comparison of ^{14}N HYSCORE spectra: WT protein (red) and L223SA mutant (blue) in H_2O (magnetic field of 345.6 mT, τ of 136 ns, 9.690 GHz). Cross-peaks 1 are produced by the N_δ atom of His-L190 and cross-peaks 2 by the peptide nitrogen of Gly-L225.

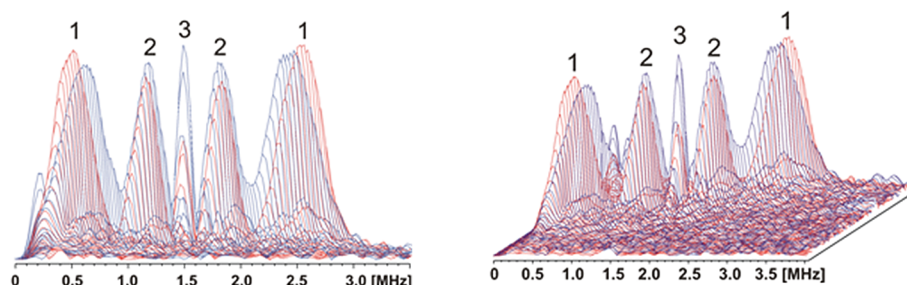
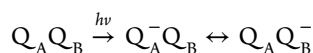


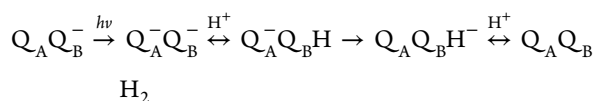
Figure 4. Comparison of ^{15}N HYSCORE spectra: ^{15}N uniformly labeled WT protein (red) and L223SA mutant (blue) in H_2O (magnetic field of 345.0 mT, τ of 200 ns, 9.6871 GHz). Cross-peaks 1 are produced by the N_δ atom of His-L190 and cross-peaks 2 by the peptide nitrogen of Gly-L225.

RCs singly mutated in this manner (Ala-M260 \rightarrow Trp), the X-ray crystal structure shows that a chloride ion is bound in the empty Q_A site.²⁸ It is easy to imagine that the presence of this anion could mimic the state with Q_A^- present, thereby elevating the pK_a of Q_B^- .

Implications for the Role of Ser-L223 in Q_B Protonation. The absence of a hydrogen bond from Ser-L223 to Q_B^- , as demonstrated here, is in agreement with previous conclusions drawn from FTIR studies.¹² It is also in accord with the finding that the rate of the first electron transfer, from Q_A^- to Q_B , is not dependent on the identity of the residue at position L223.²⁹



The conclusion is that Ser-L223 does not donate a hydrogen bond to the semiquinone Q_B^- species generated after the first flash. However, the residue is known to significantly influence the rate of reaction and proton transfer associated with the second electron transfer step, i.e., from Q_A^- to Q_B^- .²⁸



The Ser-L223 \rightarrow Ala mutant is fully inhibited in the proton-activated transfer of the second electron Q_B^- ,²⁹ indicative of the complete fracture of the proton delivery pathway to O_1 of the semiquinone. It is believed, therefore, that Ser-L223 functions as the donor of the proton to the O_1 atom of Q_B^- , leading to formation of a transient neutral semiquinone, $\text{Q}_\text{B}\text{H}$, prior to the acceptance of a second electron from Q_A^- to form $\text{Q}_\text{B}\text{H}^-$.^{1,2,29} However, in the $\text{Q}_\text{A}\text{Q}_\text{B}^-$ state observed in this work, no hydrogen bond is formed between Ser-L223 and Q_B^- ; instead, Ser-L223 is likely to be hydrogen bonded to the carboxylate group of Asp-L213 after the first flash. Following the second

flash, formation of the $\text{Q}_\text{A}^-\text{Q}_\text{B}^-$ state likely promotes formation of a hydrogen bond from Ser-L223 to Q_B^- facilitating proton donation. The pK_a of Q^-/QH in vitro has been estimated^{30,31} to be in the range of 4–6, but the doubly negatively charged state, $\text{Q}_\text{A}^-\text{Q}_\text{B}^-$, can be expected to have an increased pK_a value for both Q_A^- and Q_B^- . Elevation of this value for Q_B^- may favor cleavage of the hydrogen bond from Ser-L223 to Asp-L213 and rotation of the hydroxyl group to hydrogen bond to Q_B^- . This sets the stage for formation of $\text{Q}_\text{B}\text{H}$, accompanied by the influx of protons from the bulk phase (the periplasm, in vivo) via a chain of proton acceptors leading to Ser-L223 via the Asp-L213 residue, and restoration of the original hydrogen bonding interaction between the serine and aspartate. The subsequent transfer of an electron from Q_A^- to $\text{Q}_\text{B}\text{H}$ and the uptake of another proton at the O_4 atom lead to formation of $\text{Q}_\text{B}\text{H}_2$. The quinol can then diffuse out of the site and be replaced by another quinone molecule from the pool.

CONCLUSIONS

ENDOR and ESEEM data show that the spectroscopic differences between the mutant L223SA and WT samples are negligible, indicating minor perturbations in the SQ_B spin density for the mutant sample. Qualitatively, this suggests that, after the first flash, a strong hydrogen bond does not exist in the WT between the Ser-L223 hydroxyl group and the SQ_B O_1 atom, as removal of this hydrogen bond in the mutant should cause a significant redistribution of the spin density of the semiquinone reflected in altered hyperfine couplings. We show quantitatively, using QM/MM calculations, that a WT model in which the Ser-L223 hydroxyl group is rotated to prevent the formation of a hydrogen bond with the SQ_B O_1 atom predicts negligible change for the L223SA mutant. This, together with the better agreement between key QM/MM calculated and experimental hfcs for the non-hydrogen-bonded model, leads

us to conclude that no strong hydrogen bond exists between the Ser-L223 hydroxyl group and the SQ_B O₁ atom in the WT after the first flash.

■ ASSOCIATED CONTENT

■ Supporting Information

One-dimensional four-pulse ESEEM, ²H HYSCORE, ¹⁴N HYSCORE, ¹⁵N HYSCORE, and Field Swept ESE spectra for WT and SL223A samples. This material is available free of charge via the Internet at <http://pubs.acs.org>.

■ AUTHOR INFORMATION

Corresponding Author

*P.J.O.: e-mail, patrick.omalley@manchester.ac.uk; phone, 00441612004536. S.A.D.: e-mail, dikanov@illinois.edu; phone, (217) 300-2209. C.A.W.: e-mail, cwraight@illinois.edu; phone, (217) 333-1630.

Present Address

@St. Jude Children's Research Hospital, Memphis, TN 38105.

Funding

This investigation was supported by National Institutes of Health Grant GM062954 and Grant DE-FG02-08ER15960 from the Chemical Sciences, Geosciences and Biosciences Division, Office of Basic Energy Sciences, Office of Sciences, U.S. Department of Energy (S.A.D.), National Science Foundation Grant MCB-0818121 (C.A.W.), and National Center for Research Resources Grants S10-RR15878 and S10-RR025438 for pulsed EPR instrumentation. P.J.O. acknowledges the use of computer resources granted by the EPSRC UK national service for computational chemistry software (NSCCS).

Notes

The authors declare no competing financial interest.

■ ABBREVIATIONS

DFT, density functional theory; B3LYP, Becke3 Lee–Yang–Parr; QM, quantum mechanics; MM, molecular mechanics; SQ, semiquinone; RC, reaction center; ONIOM, Our Own N-layered Integrated Molecular Orbital and Molecular Mechanics; EPR, electron paramagnetic resonance; ENDOR, electron nuclear double-resonance; ESEEM, electron spin echo envelope modulation; HYSCORE, hyperfine sublevel correlation; hfc, hyperfine coupling constant.

■ REFERENCES

- (1) Wraight, C. A. (2004) Proton and electron transfer in the acceptor quinone complex of photosynthetic reaction centers from *Rhodobacter sphaeroides*. *Front. Biosci.* 9, 309–337.
- (2) Okamura, M. Y., Paddock, M. L., Graige, M. S., and Feher, G. (2000) Proton and electron transfer in bacterial reaction centers. *Biochim. Biophys. Acta* 1458, 148–163.
- (3) Crofts, A. R. (2004) The cytochrome *bc*₁ complex: Function in the context of structure. *Annu. Rev. Physiol.* 66, 689–733.
- (4) Lancaster, C. R. D., and Michel, H. (1997) The coupling of light-induced electron transfer and proton uptake as derived from crystal structures of reaction centers from *Rhodospseudomonas viridis* modified at the binding site of the secondary quinone, Q_B. *Structure* 5, 1339–1359.
- (5) Ermler, U., Fritzsche, G., Buchanan, S. K., and Michel, H. (1994) Structure of the photosynthetic reaction center from *Rhodobacter sphaeroides* at 2.65 Å resolution: Cofactors and protein-cofactor interactions. *Structure* 2, 925–936.

(6) Stowell, M. H. B., McPhillips, T. M., Rees, D. C., Solitis, S. M., Abresch, E., and Feher, G. (1997) Light-induced structural changes in photosynthetic reaction center: Implications for mechanism of electron-proton transfer. *Science* 276, 812–816.

(7) Lubitz, W., and Feher, G. (1999) The primary and secondary acceptors in bacterial photosynthesis III. Characterization of the quinone radicals Q_A^{•−} and Q_B^{•−} by EPR and ENDOR. *Appl. Magn. Reson.* 17, 1–48.

(8) Nabedryk, E., Breton, J., Hienerwadel, R., Fogel, C., Mantele, W., Paddock, M. L., and Okamura, M. Y. (1995) FTIR spectroscopy of Q_B photoreduction in *Rb. sphaeroides* reaction centers: Effects of site-directed replacements at Glu-L212, Asp-L213, and Asp-L210 and of ¹H/²H exchange. *Photosynthesis: From Light to Biosphere*, Vol. I, pp 875–878.

(9) Graige, M. S., Feher, G., and Okamura, M. Y. (1998) Conformational gating of the electron transfer reaction Q_A^{•−}Q_B → Q_AQ_B^{•−} in bacterial reaction centers of *Rhodobacter sphaeroides* determined by a driving force assay. *Proc. Natl. Acad. Sci. U.S.A.* 95, 11679–11684.

(10) Koepke, J., Krammer, E. M., Klinge, A. R., Sebban, P., Ullmann, G. M., and Fritzsche, G. (2007) pH modulates the quinone position in the photosynthetic reaction center from *Rhodobacter sphaeroides* in the neutral and charge separated states. *J. Mol. Biol.* 371, 396–409.

(11) Alexov, E., Miksovskaya, J., Baciou, L., Schiffer, M., Hanson, D. K., Sebban, P., and Gunner, M. R. (2000) Modeling the Effects of Mutations on the Free Energy of the First Electron Transfer from Q_A to Q_B in Photosynthetic Reaction Centers. *Biochemistry* 39, 5940–5952.

(12) Nabedryk, E., Paddock, M. L., Okamura, M. Y., and Breton, J. (2005) An isotope-edited FTIR investigation of the role of Ser-L223 in binding quinone (Q_B) and semiquinone (Q_B^{•−}) in the reaction center from *Rhodobacter sphaeroides*. *Biochemistry* 44, 14519–14527.

(13) Paddock, M. L., Flores, M., Isaacson, R., Chang, C., Abresch, E. C., and Okamura, M. Y. (2007) ENDOR spectroscopy reveals light induced movement of the H-bond from Ser-L223 upon forming the semiquinone (Q_B^{•−}) in reaction centers from *Rhodobacter sphaeroides*. *Biochemistry* 46, 8234–8243.

(14) Takahashi, E., Maróti, P., and Wraight, C. A. (1990) Site-directed mutagenesis of *Rhodobacter sphaeroides* reaction centers: The role of Tyr^{L222}. In *Current Research in Photosynthesis* (Baltscheffsky, M., Ed.) Vol. 1, pp 169–172, Kluwer Academic Publishers, Dordrecht, The Netherlands.

(15) Takahashi, E., and Wraight, C. A. (2006) Small weak acids reactivate proton transfer in reaction centers from *Rhodobacter sphaeroides* mutated at Asp^{L210} and Asp^{M17}. *J. Biol. Chem.* 281, 4413–4422.

(16) Goldsmith, J. O., and Boxer, S. G. (1996) Rapid isolation of bacterial photosynthetic reaction centers with an engineered poly-histidine tag. *Biochim. Biophys. Acta* 1276, 171–175.

(17) Martin, E., Samoilova, R. I., Narasimhulu, K. V., Wraight, C. A., and Dikanov, S. A. (2010) Hydrogen bonds between nitrogen donors and the semiquinone in the Q_B site of bacterial reaction centers. *J. Am. Chem. Soc.* 132, 11671–11677.

(18) Martin, E., Samoilova, R. I., Narasimhulu, K. V., Lin, T. J., O'Malley, P. J., Wraight, C. A., and Dikanov, S. A. (2011) Hydrogen Bonding and Spin Density Distribution in the Q_B Semiquinone of Bacterial Reaction Centers and Comparison with the Q_A Site. *J. Am. Chem. Soc.* 133, 5525–5537.

(19) Schweiger, A., and Jeschke, G. (2001) *Principles of pulse electron paramagnetic resonance*, Oxford University Press, Oxford, U.K.

(20) Axelrod, H. L., Abresch, E. C., Paddock, M. L., Okamura, M. Y., and Feher, G. (2000) Determination of the binding sites of the proton transfer inhibitors Cd²⁺ and Zn²⁺ in bacterial reaction centers. *Proc. Natl. Acad. Sci. U.S.A.* 97, 1542–1547.

(21) Vreven, T., Byun, K. S., Komaromi, I., Dapprich, S., Montgomery, J. A., Morokuma, K., and Frisch, M. J. (2006) Combining quantum mechanics methods with molecular mechanics methods in ONIOM. *J. Chem. Theory Comput.* 2, 815–826.

(22) Frisch, M. J., Trucks, G. W., Schlegel, H. B., Scuseria, G. E., Robb, M. A., Cheeseman, J. R., Scalmani, G., Barone, V., Mennucci, B., Petersson, G. A., Nakatsuji, H., Caricato, M., Li, X., Hratchian, H. P., Izmaylov, A. F., Bloino, J., Zheng, G., Sonnenberg, J. L., Hada, M., Ehara, M., Toyota, K., Fukuda, R., Hasegawa, J., Ishida, M., Nakajima, T., Honda, Y., Kitao, O., Nakai, H., Vreven, T., Montgomery, J. A., Jr., Peralta, J. E., Ogliaro, F., Bearpark, M., Heyd, J. J., Brothers, E., Kudin, K. N., Staroverov, V. N., Kobayashi, R., Normand, J., Raghavachari, K., Rendell, A., Burant, J. C., Iyengar, S. S., Tomasi, J., Cossi, M., Rega, N., Millam, J. M., Klene, M., Knox, J. E., Cross, J. B., Bakken, V., Adamo, C., Jaramillo, J., Gomperts, R., Stratmann, R. E., Yazyev, O., Austin, A. J., Cammi, R., Pomelli, C., Ochterski, J. W., Martin, R. L., Morokuma, K., Zakrzewski, V. G., Voth, G. A., Salvador, P., Dannenberg, J. J., Dapprich, S., Daniels, A. D., Farkas, Ö., Foresman, J. B., Ortiz, J. V., Cioslowski, J., and Fox, D. J. (2009) *Gaussian 09*, revision A.1, Gaussian, Inc., Wallingford, CT.

(23) O'Malley, P. J. (1996) ^1H , ^{13}C and ^{17}O principal hyperfine tensor determination for the *p*-benzosemiquinone anion radical using hybrid density functional methods. *Chem. Phys. Lett.* 262, 797–800.

(24) O'Malley, P. J. (1997) A Hybrid Density Functional Study of the *p*-Benzosemiquinone Anion Radical: The Influence of Hydrogen Bonding on Geometry and Hyperfine Couplings. *J. Phys. Chem. A* 101, 6334–6338.

(25) Niklas, J., Epel, B., Antonkine, M. L., Sinnecker, S., Pandelia, M. E., and Lubitz, W. (2009) Electronic Structure of the Quinone Radical Anion A_1^- of Photosystem I Investigated by Advanced Pulse EPR and ENDOR Techniques. *J. Phys. Chem. B* 113, 10367–10379.

(26) Lin, T. J., and O'Malley, P. J. (2011) Binding Site Influence on the Electronic Structure and Electron Paramagnetic Resonance Properties of the Phyllosemiquinone Free Radical of Photosystem I. *J. Phys. Chem. B* 115, 9311–9319.

(27) Paddock, M. L., Flores, M., Isaacson, R., Shepherd, J. N., and Okamura, M. Y. (2010) EPR and ENDOR Investigation of Rhodosemiquinone in Bacterial Reaction Centers Formed by B-Branch Electron Transfer. *Appl. Magn. Reson.* 37, 39–48.

(28) McAuley, K. E., Fyfe, P. K., Ridge, J. P., Cogdell, R. J., Isaacs, N. W., and Jones, M. R. (2000) Ubiquinone binding, ubiquinone exclusion, and detailed cofactor conformation in a mutant bacterial reaction center. *Biochemistry* 39, 15032–15043.

(29) Paddock, M. L., McPherson, P. H., Feher, G., and Okamura, M. Y. (1990) Pathway of proton transfer in bacterial reaction centers: Replacement of serine-L223 with alanine inhibits electron and proton transfers associated with reduction of quinone to dihydroquinone. *Proc. Natl. Acad. Sci. U.S.A.* 87, 6803–6807.

(30) Land, E. J., and Swallow, A. J. (1970) One-Electron Reactions in Biochemical Systems as Studied by Pulse Radiolysis. 3. Ubiquinone. *J. Biol. Chem.* 245, 1890–1897.

(31) Morrison, L. E., Schelhorn, J. E., Cotton, T. M., and Loach, P. A. (1982) in *The Function of Quinones in Energy Conserving Systems* (Trumpower, B. L., Ed.) pp 35–58, Academic, New York.